The influence of interfacial barrier engineering on the resistance switching of In_2O_3:SnO_2/TiO_2/In_2O_3:SnO_2 device*

Liu Zi-Yu(刘紫玉), Zhang Pei-Jian(张培健), Meng Yang(孟 洋), Li Dong(李 栋), Meng Qing-Yu(孟庆宇), Li Jian-Qi(李建奇), and Zhao Hong-Wu(赵宏武)†

Beijing National Laboratory for Condensed Matter Physics, Institute of Physics, Chinese Academy of Sciences, Beijing 100190, *China*

(Received 28 October 2011; revised manuscript received 9 November 2011)

The I–V characteristics of In_2O_3:SnO_2/TiO_2/In_2O_3:SnO_2 junctions with different interfacial barriers are investigated by comparing experiments. A two-step resistance switching process is found for samples with two interfacial barriers produced by specific thermal treatment on the interfaces. The nonsynchronous occurrence of conducting filament formation through the oxide bulk and the reduction in the interfacial barrier due to the migration of oxygen vacancies under the electric field is supposed to explain the two-step resistive switching process. The unique switching properties of the device, based on interfacial barrier engineering, could be exploited for novel applications in nonvolatile memory devices.

Keywords: resistance switching, interfacial Schottky barrier, oxygen vacancy, two-step switching

PACS: 73.40.–c, 73.50.–h **DOI:** 10.1088/1674-1056/21/4/047302

1. Introduction

Resistance switching (RS) in metal/oxide/metal thin films has been studied extensively for its potential applications in high density memory devices.[1−3] The role of the interfacial structure between electrodes and oxides has attracted considerable attention for the understanding of the switching mechanism. Several groups[4−6] have reported that the "interfacial transition layer" formed by redox reactions at the metal/oxide interface plays an important role in the RS process, while Blom *et al.*[7] and Sawa *et al.*[8] believed that one of the most important features during RS is the electric-field-induced variation of Schottky barrier height near the metal–oxide interface. Jeong *et al.*[9] and Lee *et al.*[10] found that RS characteristics, such as endurance performance, can be enhanced by introducing an ultrathin layer into the interface region. Furthermore, both filamentary switching and homogenous interfacial switching at the metal–oxide interface have been reported to coexist in one sample and exhibit the opposite switching behaviours.[11] At the metal–oxide interface, however, the improper concentration of oxygen–vacancy defects always leads to an irreversible resistance change for memory application. Moreover, the absence of effectively controlled doping of oxygen vacancies makes it difficult to resolve the interface issues. Therefore, a systematic investigation of interfacial RS by controlling oxygen vacancies is beneficial to understanding the RS mechanism and further realizing memory devices with high performance.

In this paper, we investigate the RS characteristics of In_2O_3:SnO_2(ITO)/TiO_2/ITO junctions with different interfacial structures through specific thermal treatment toward interfaces with TiO_2 in the oxygen atmosphere. Through comparing experiments, a two-step resistance switching process is found for samples with two interfacial barriers. The RS mechanism is ascribed to the formation and rupture of conducting paths penetrating through the whole sample due to the migration of oxygen vacancies. The nonsynchronous occurrence of conducting filament formation through the oxide bulk and the reduction in the inter-

*Project supported by the National Basic Research Program of China (Grant No. 2009CB930803), the National Natural Science Foundation of China (Grant No. 10834012), and the Innovation Foundation of the Chinese Academy of Sciences (Grant No. KJCX2-YW-W24).

†Corresponding author. E-mail: hwzhao@iphy.ac.cn

© 2012 Chinese Physical Society and IOP Publishing Ltd

facial barrier plays an important role in the two-step RS process.

2. Experimental procedure

The sample preparation details in our experiments have been reported previously.[4,12] The sandwiched structure of ITO/TiO_2/ITO was deposited by RF magnetron sputtering on commercial glass substrates. The oxide targets were used for ITO and TiO_2, separately. The ITO bottom electrode (BE) of 400 nm in thickness was prepared at ambient temperature (AT) in an Ar pressure of 0.6 Pa, followed by annealing at 400 °C for 10 min under an O_2 pressure of 0.33 Pa. Without breaking vacuum, the TiO_2 films 100 nm in thickness were grown subsequently at AT. Three totally different specimens of TiO_2 films were prepared by specific thermal treatments, as schematized in Fig. 1(a). For sample A, the TiO_2 film was further treated by annealing at 400 °C in an O_2 atmosphere of 0.33 Pa for 10 min after the deposition at AT. For sample B, the same annealing process was carried out for the first deposited TiO_2 film of 5 nm thickness, then the remaining TiO_2 film of 95 nm was deposited at AT. For sample C, the TiO_2 film of 100 nm was prepared at AT without any annealing process. Then, the ITO top electrode (TE) of 50 nm in thickness was prepared under the same conditions as that for the bottom ITO film. Finally, the sample was covered by a 20-nm Au film to protect it from contamination. An array of TE pads with an area of 80 μm×80 μm was fabricated using a conventional photolithography technique. Keithley 2400 and 2182 instruments were used for the pulsed I–V characterizations, and high-resolution transmission electron microscopy (HRTEM) was employed to investigate the interfacial structure of the samples.

3. Results and discussion

Figures 1(b) and 1(c) show HRTEM images of the cross sectional view of samples A and B, respectively. Although the top interface of the TiO_2 film of sample A and the bottom interface of the TiO_2 film of sample B were treated by a special annealing process, no significant difference in interfacial microstructure between the two samples is observed. A similar HRTEM result is observed for sample C, which shows negligible variation of interfacial microstructure resulting from the thermal treatment toward the interfaces (not shown here) compared with samples A and B.

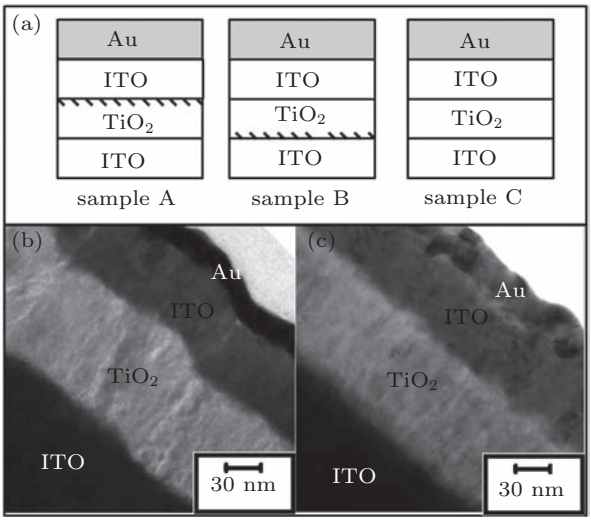


Fig. 1. (a) Schematics of samples A, B, and C. The shadow region represents the annealed TiO_2 interface. (b) HRTEM images of the cross sectional view of sample A. (c) HRTEM images of the cross sectional view of sample B.

For all electrical measurements, the BE was grounded and the TE was always biased. The pulsed voltage was scanned from $0 \rightarrow +V_{max} \rightarrow -V_{max} \rightarrow 0$. The initial current–voltage (I–V) curve of sample A in its virgin state exhibits a strong rectifying characteristic similar to that observed for the Pt/TiO_2/Pt structure[13–15] as shown in Fig. 2(a). This is a typical feature of the reversed Schottky barrier. For sample B, in contrast, a symmetric nonlinear I–V characteristic shows up with extremely large resistance at both positive and negative bias voltages, revealing the existence of two Schottky barriers with opposite polarities. The I–V curve of sample C is similar to that of sample B with larger resistance, revealing a similar configuration of two opposite Schottky junctions with larger barrier height. Note that the structure difference between samples A and C is that the top interface of the TiO_2 film of sample A was annealed in the oxygen atmosphere. Since the oxygen pressure of 0.33 Pa is extremely low, the annealing process was almost performed in the vacuum, and therefore the annealing process creates an oxygen-deficient layer near the TiO_2 surface,[13] which collapses the Shottky barrier and leads to the formation of the Ohmic contact at the top TiO_2 interface of sample A. Actually, oxygen vacancies in TiO_2 are known to act as n-type dopants,[16] which converts the insulating oxide into

an electrically conductive doped semiconductor and serves as the Ohmic metal/oxide contact structure.[17] For sample B, although the TiO_2 layer near the bottom interface was also treated by an annealing process in the oxygen atmosphere, a Schottky barrier still exists at the bottom interface, as shown in Fig. 2(a). The reason for this is still not clear, and further investigations are needed to resolve the issue.

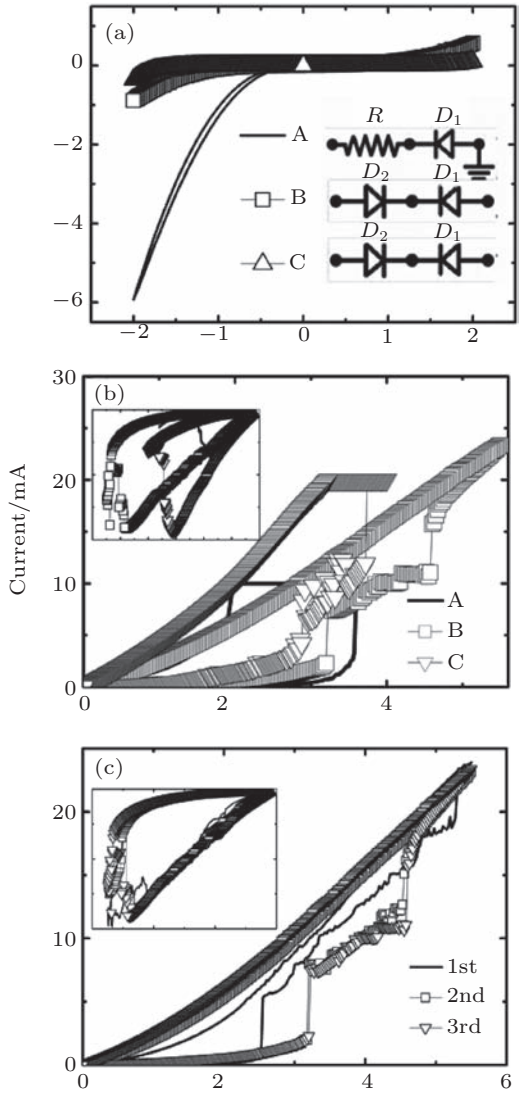


Fig. 2. (a) The I–V characteristics of samples A, B, and C; the insets show the corresponding equivalent circuit diagrams consisting of two electronic elements (rectifier or resistor) in series. (b) The switching curves of samples A, B, and C at positive bias voltage; the inset shows the switching curves at negative bias voltage. (c) The repeatable two-step switching behaviour of sample B; the inset indicates the switching curves at negative bias voltage.

Figure 2(b) shows the I–V characteristics of the above samples after the forming process. For sample A, the RS effect occurs from the high resistance state (HRS) to the low resistance state (LRS) as the positive bias voltage reaches 3.6 V with a current compliance of 10 mA to protect the device from breaking down, and the device can be switched back to the HRS by applying a negative bias (shown in the inset). For comparison, the I–V curve of sample B exhibits a two-step switching phenomenon. Firstly, the current rises sharply at about 2.5 V (defined as V_1), generating an intermediate resistance state (IRS). Secondly, with the applied voltage increasing further, the current increases significantly at about 4.6 V (defined as V_2), leading to RS from IRS to LRS. The LRS can be directly switched back to HRS by applying a negative bias. During the two-step switching, a current compliance of 20 mA is fixed to protect the sample from breaking down. The two-step switching behaviour is repeatable for sample B, as shown in Fig. 2(c). By comparison, the two-step process is not observed for sample A, even if we increase the current compliance up to 20 mA or more. A similar two-step switching effect is exhibited for sample C with different values of switching voltage ($V_1 = 2.8$ V, $V_2 = 3.8$ V). As a whole, samples B and C need a higher voltage to complete the switching from HRS to LRS, and the switching process shows a special two-step behaviour.

To further understand the two-step switching mechanism, we gradually increased the sweep voltage range $V_{\max}$ so as to explore the electroforming process under different electric fields. For sample A, the I–V curve maintains a strongly rectifying behaviour until $V_{\max}$ reaches 3.5 V, as shown in Fig. 3(a). As $V_{\max}$ exceeds $V_C = 3.5$ V, the I–V curve quickly evolves into a bipolar RS behaviour. For sample B, the I–V curve maintains a symmetric nonlinear characteristic with extremely high resistance until $V_{\max}$ reaches $V_{C1} = 3$ V, see Fig. 3(b). Further increasing the bias up to 4 V leads to a small I–V loop, but the current will fall into the same trace as the bias decreases. When $V_{\max}$ exceeds $V_{C2} = 5$ V, the I–V curve exhibits a two-step switching effect, as shown in Fig. 3(b). The same trend is observed for sample C with a slightly different switching voltage.

From the above observations of Figs. 2 and 3, we conclude that the electroforming process and the two-step RS process in TiO_2 are influenced by the interfacial barriers and the applied voltage, as indicated in Fig. 4. Moreover, we discuss the RS mechanism of TiO_2 influenced by interfacial structure under three different conditions: i) the RS process of sample A, ii) the I–V characteristics of sample B under small electric fields, and iii) the two-step RS process of sample B.

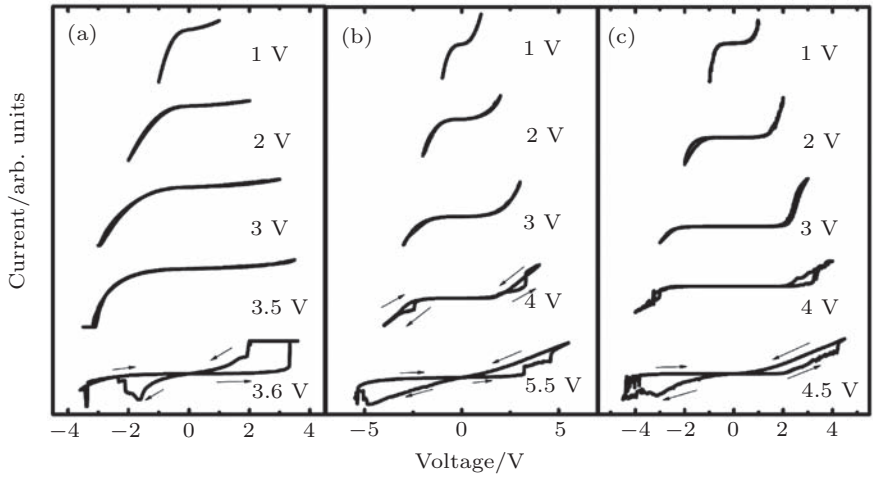


Fig. 3. The evolution of the I–V characteristics for (a) sample A, (b) sample B, and (c) sample C, when the applied pulse voltage sweeping is from 0 V$\rightarrow V_{\max} \rightarrow$ 0 V $\rightarrow -V_{\max} \rightarrow$ 0 V.

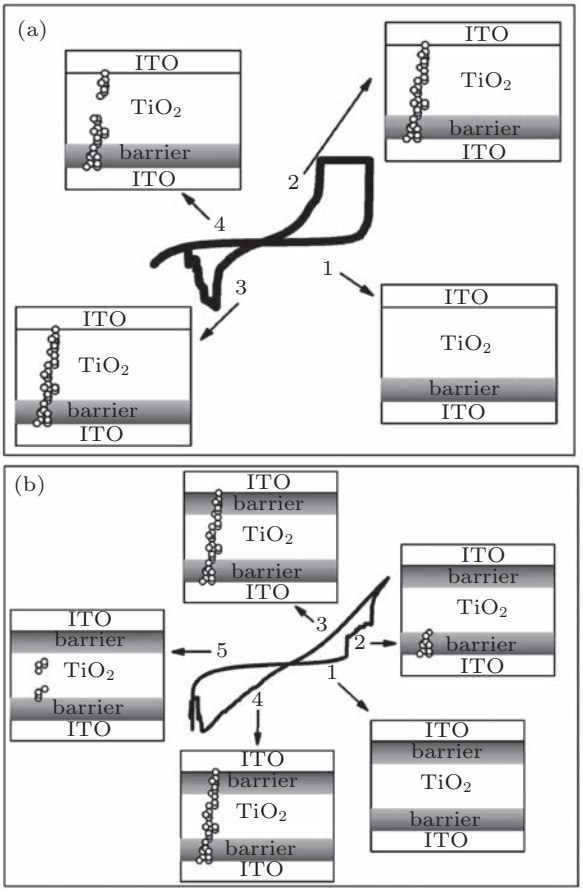


Fig. 4. Diagrams of the switching mechanism for (a) sample A and (b) sample B.

(i) For sample A, the switching characteristics are similar to those reported previously and can be described as the formation and the rupture of the filamentary conductive paths in the TiO_2 bulk via the migration of oxygen vacancies under electric field,[12,18,19] as displayed in Fig. 4(a). During formation, a positive voltage applied to the TE produces a large voltage drop at the reverse-biased Schottky barrier D_1 near the BE, see Fig. 2(a). Hence positively charged oxygen vacancies are likely to drift toward the BE and accumulate there until their doping effect reduces the electronic barrier to a conductive level and forms conducting paths through the TiO_2 film. After the formation process, both the resistive TiO_2 bulk and the barrier D_1 are penetrated by conductive channels almost simultaneously, creating the LRS. When a negative bias is applied, the oxygen vacancies drift back and the conducting channel is interrupted, leading to the HRS.[18,19] Moreover, Schottky barrier D_1 is unrecoverable in sample A once electroforming is completed.

(ii) For sample B, the existence of two interfacial barriers results in a totally different switching process, as shown in Fig. 3(b). Firstly, when a small positive voltage is applied, the forward-biased Schottky barrier D_2 is relatively conductive and the voltage drop is concentrated across the reverse-biased D_1 near the BE. Thereafter, positively charged oxygen vacancies are likely to be created near the BE at first, and be accumulated so as to reduce the electronic barrier D_1 to a conductive level at $V = V_1$. However, due to the different thermal treatments on the bottom interface of the TiO_2 film, there is now no conducting path formed through the oxide bulk in sample B, which is contrary to what happens in sample A. Thus, the absence of conductive filaments will result in an IRS, instead of an LRS. Subsequently reducing the applied voltage will then lead to the current falling into the same trace, generating the small I–V loop as described

previously in Fig. 2(b). On the other hand, when a small negative voltage is applied, the top barrier D_2 is reverse-biased and the accumulated oxygen vacancies will destroy D_2 as the voltage increases, hence showing a similar small I–V loop in the negative bias range. Meanwhile, the bottom barrier D_1 is recovered due to the fact that the oxygen vacancies near the BE drift toward the TE under the electric field. In a word, under a smaller electric field, sample B only shows the rectifying characteristic of one Schottky barrier in series with the resistance of the TiO_2 bulk, and there are no conducting filaments formed through the oxide.

(iii) When the positive voltage applied to sample B increases and exceeds V_2, a large number of oxygen vacancies will be accumulated through the oxide bulk and lead to the formation of the conducting filaments starting from the BE and heading for the TE, as depicted in Fig. 4(b). Meanwhile, a large number of oxygen vacancies are aggregated around the BE/TiO_2 interface and cannot be annihilated by the external oxygen or oxygen ions inside the ITO TE. Therefore, the top barrier D_2 is penetrated by the accumulated oxygen vacancies,[13,18] and as a result conductive filaments are formed through the TiO_2 bulk and at two interfacials, resulting in the second resistance changing from IRS to LRS. In the case where a negative voltage is applied to sample B, the oxygen vacancies are repelled to migrate toward the TE. Hence, the barrier D_1 near the BE is restored and the conductive filaments across the oxide bulk are correspondingly interrupted. Meanwhile, the barrier D_2 near the TE is recovered due to the chemical reaction of oxygen vacancies at the TE/oxide interface with oxygen gas molecules in air.[20] All these processes have combined to create the RS from LRS to HRS. Conclusively, the nonsynchronous occurrence of conducting filament formation through the oxide bulk and the reduction in the interfacial barrier leads to the special two-step RS process for sample B with two interfacial barriers. A similar RS mechanism is applied to sample C, which exhibits two-step RS behaviour. Due to the difference in the interfacial barriers produced during device fabrication, the critical switching voltages V_1 and V_2 of sample C are lower than those of sample B.

4. Conclusion

We investigated the RS characteristics of ITO/TiO_2/ITO junctions with different interfacial barriers by comparing experiments. The samples with two interfacial barriers produced by specifically thermal treatment on the interface exhibit a two-step resistance switching behaviour. The RS mechanism is ascribed to the formation and rupture of conducting paths penetrating the whole sample due to the migration of oxygen vacancies. The nonsynchronous occurrence of conducting filament formation through the oxide bulk, and the reduction in the interfacial barrier, is supposed to interpret the two-step RS process. These results, based on interfacial barrier engineering, should be applicable to all resistive oxide switching devices.

References

[1] Waser R and Aono M 2007 *Nature Materials* **6** 833

[2] Sawa A 2008 *Materials Today* **11** 28

[3] Kyung Min Kim, Doo Seok Jeong and Cheol Seong Hwang 2011 *Nanotechnology* **22** 254002

[4] Liao Z L, Wang Z Z, Meng Y, Liu Z Y, Gao P, Gang J L, Zhao H W, Liang X J, Bai X D and Chen D M 2009 *Appl. Phys. Lett.* **94** 253503

[5] Li Y, Zhao G Y, Su J, Shen E F and Ren Y 2011 *Appl. Phys.* A **104** 1069-1073

[6] Oh S C, Jung H Y and Lee H 2011 *J. Appl. Phys.* **109** 124511

[7] Blom P W M, Wolf R M, Cillessen J F M and Krijin M P C M 1994 *Phys. Rev. Lett.* **73** 2107

[8] Sawa A, Fujii T, Kawasaki M and Tukura Y 2004 *Appl. Phys. Lett.* **85** 4073

[9] Jeong H Y, Lee J Y and Choi S Y 2010 *Adv. Funct. Mater.* **20** 3912

[10] Lee M D, Ho C H and Yao Y D 2011 *IEEE Transactions on Magnetic* **47** 3

[11] Muenstermann R, Menke T, Dittmann R and Waser R 2010 *Adv. Mater.* **22** 4819

[12] Meng Y, Zhang P J, Liu Z Y, Liao Z L, Pan X Y, Liang X J, Zhao H W and Chen D M 2010 *Chin. Phys.* B **19** 037304

[13] Yang J J, Pickett M D, Li X, Ohlberg D A A, Stewart D R and Williams R S 2008 *Nanotechnol.* **3** 429

[14] Chung Y L, Lai P Y, Chen Y C and Chen J S 2011 *Appl. Mater. Interfaces* **3** 1918

[15] Park W Y, Kim G H, Seok J Y, Kim K M, Song S J, Lee M H and Hwang C S 2010 *Nanotechnology* **21** 195201

[16] Knauth P and Tuller H L 1999 *J. Appl. Phys.* **85** 897

[17] Rhoderick E H and Williams R H 1988 *Metal–Semiconductor Contacts* 2nd edn. (Oxford: Clarendon)

[18] Yang J J, Miao F, Pickett M D, Ohlberg D A A, Stewart D R, Lau C N and William R S 2009 *Nanotechnology* **20** 215201

[19] Miao F, Yang J J and Borghetti J 2011 *Nanotechnology* **22** 254007

[20] Jeong D S, Schroeder H, Breuer U and Waser R 2008 *J. Appl. Phys.* **104** 123716